Origin of deep localization in $GaAs_{1-x}Bi_x$ and its consequences for alloy properties

K. Alberi,[1] B. Fluegel,[1] D. A. Beaton,[1] M. Steger,[1] S. A. Crooker,[2] and A. Mascarenhas[1]
[1]*National Renewable Energy Laboratory, Golden, Colorado 80401, USA*
[2]*National High Magnetic Field Laboratory, Los Alamos National Laboratory, Los Alamos, New Mexico 87545, USA*

(Received 12 July 2018; revised manuscript received 27 September 2018; published 28 November 2018)

The addition of Bi isoelectronic dopants to GaAs provides an attractive avenue for tailoring its electronic band structure, yet it also introduces less appealing and very strong hole localization. The origin of the localization is still not thoroughly understood, which has in part inhibited the practical use of $GaAs_{1-x}Bi_x$ alloys. In this study, the evolution of hole localization was evaluated as a function of composition. We find that spatial overlap of Bi-related bound states at concentrations >0.6% Bi effectively enables holes to be channeled to those at the lowest energies, thereby aiding localization of excitons ⩾150 meV below the band gap. The large energy gap between these bound states and the GaAs valence-band edge combined with the slow upward movement of the valence band with composition causes deep localization to persist to high concentrations >6% Bi. The results provide important insight into the optical and transport behavior of $GaAs_{1-x}Bi_x$ and its implications for device applications.

DOI: 10.1103/PhysRevMaterials.2.114603

I. INTRODUCTION

Tailoring semiconductor properties through alloying is routinely employed in semiconductor engineering. Utilizing highly electronegative/electropositive alloy substituents, also referred to as isoelectronic impurities, amplifies the degree to which those properties can be modified. For example, substitution of just 1 at. % of the As atoms in GaAs with more electronegative N reduces the band gap by 180 meV [1–3]. Incorporating the same concentration of electropositive Bi results in a band gap reduction of 88 meV and an increase in the spin-orbit splitting energy by nearly the same amount [4,5]. The advantage of this approach is that large changes to the host band structure can be generated with only a small change in the alloy composition. Dilute nitride and bismide alloys have therefore been advertised as the next generation of semiconductors for near-infrared optoelectronic devices that can be built on closely lattice-matched conventional substrates [6].

Despite these promising attributes, isoelectronic impurities also introduce a high degree of carrier scattering and localization that have thus far limited their use in practical applications [7]. Carrier localization has been most extensively studied in $GaAs_{1-x}N_x$ [8–10]. While the state associated with an isolated N atom is resonant within the conduction band, stochastic location of two or more N atoms near one another in the lattice produces bound states below the conduction-band edge (CBE) that act as deep electron traps. Their evolution with composition has been studied optically in $GaAs_{1-x}N_x$ samples with N concentrations ranging from 0.001 to 1% [8,11,12]. Excitonic wave-function overlap of two or more N-related bound states starting at ∼0.2% N facilitates tunneling, hopping, and diffusion [13] (otherwise known as energy transfer) of electrons to the lowest-energy bound states, leading to broad photoluminescence (PL) emission with a peak that persists ∼50 meV below the band gap for concentrations ⩾0.4% N. Thus, some degree of electron localization is expected in the dilute limit and cannot be eliminated simply by improving synthesis conditions or reducing native defects in the crystal. The evolution in the PL behavior can also be viewed as a transition from a heavily impurity-doped semiconductor to an alloy [11].

Bismuth in GaAs behaves in an analogous manner. The states of isolated Bi atoms are resonant within the valence band, whereas bound states involving two or more neighboring Bi atoms form in the band gap above the valence-band edge (VBE) [14–18]. Localization behavior is very pronounced in this alloy system and has been studied in limited sets of samples by several research groups [19–22]. Low-temperature PL from samples with 1 to 8% Bi is emitted in a broad band (typically >50 meV wide) at energies up to 150 meV below the expected alloy band gap [19–23]. These studies were instrumental in identifying the existence of localization [21], showing that localization is influenced by alloying and disorder-induced changes to the valence band [20], identifying the timescales for energy transfer between localized states [22], and exploring local strain effects on the effective mass of carriers localized around Bi pair states [23]. However, they have not yet addressed the critical questions of why localization is much deeper than that found in $GaAs_{1-x}N_x$ and why it persists to much higher Bi concentrations. The lack of information is partially due to the difficulty in incorporating low concentrations of Bi (<1%) into GaAs, which has prevented evaluation of the evolution in the overlap of Bi pair and larger cluster states as the concentration increases. It is also partially due to the increased likelihood for native defect and Bi cluster formation at the low substrate temperatures and flux ratios required for Bi incorporation during growth [24–28]. These two factors obscure the distinction of whether the extreme localization behavior is an intrinsic property of dilute bismide alloys or something

 ©2018 American Physical Society

that can be alleviated through improved crystal growth. If it is intrinsic, then identification of the point at which impurity-doped behavior transitions to alloylike behavior will provide additional guidance about which composition ranges to use in technological applications and which to avoid.

Here, we study the evolution of localization in $GaAs_{1-x}Bi_x$ alloys as a function of composition in the range 0.26 to 1.75% Bi using a combination of variable temperature, time-resolved, and magneto-PL techniques to distinguish between localized and delocalized states. Alloys with Bi concentrations <0.4% Bi exhibit narrow emission signatures from bound Bi-related states near the VBE as well as lower-energy emission associated with deeper states. Alloys with Bi concentrations >0.6% Bi exhibit a single broad emission peak well below the band gap energy. By following the evolution between those two regimes in a detailed and systematic manner, we are able to determine that PL from samples with Bi concentrations >0.8% is pinned by a very deep Bi-related bound state. By identifying the fundamental origin of the deep localization in $GaAs_{1-x}Bi_x$ we are further able to predict that localization dominated by Bi-related bound states will transition to alloy-disorder-driven localization at concentrations >6%. This insight and high-level view of localization behavior in $GaAs_{1-x}Bi_x$ importantly suggest that optoelectronic devices fabricated with $GaAs_{1-x}Bi_x$ containing roughly >6% Bi will suffer less from strong localization than those containing <6%.

II. EXPERIMENTAL

$GaAs_{1-x}Bi_x$ epilayers were grown by molecular-beam epitaxy on semi-insulating GaAs (001) substrates to a thickness of approximately 300 nm. The substrate temperature was held nominally at 350 °C, and the V/III flux ratio was set just above 1 to facilitate Bi incorporation. Details of the growth conditions are published in Ref. [29]. The Bi concentrations were verified by x-ray diffraction. Variable-temperature PL measurements were performed with a 532-nm diode-pumped solid-state laser at two different excitation powers. Time-resolved PL (TRPL) measurements were performed at 5 K with a frequency-doubled line of a Ti:sapphire laser at 410 nm (∼2.5 ps, 2 pJ/pulse). Magneto-PL measurements were performed at the National High Magnetic Field Laboratory at Los Alamos National Laboratory. The samples were held at 1.5 K and the magnetic field was swept from 0 to 60 T and back to 0 T over a time of 50 ms. PL was excited with a 515-nm solid-state laser delivered to the sample through a 550-μm-diameter optical fiber. Photoluminescence was collected back through the same fiber, and spectra were continuously acquired every 2.0 ms throughout the pulse.

III. RESULTS

Temperature and power-dependent PL measurements were performed on $GaAs_{1-x}Bi_x$ samples with Bi concentrations ranging from 0.26 to 1.75%. Representative spectra are displayed in Fig. 1. Vertical markers are placed at the expected energies of Bi-related states (T_2-T_8) at 10 K, which were previously identified in the literature following the composition dependence reported in Ref. [30]. The presence of these states indicates the high material quality of the samples [29]. The expected band gap energies for the alloys were determined from the data in Ref. [18] and are marked as E_g.

At temperatures ⩽30 K, emission from the sample with 0.30% Bi [Fig. 1(a)] primarily occurs from shallow acceptor-related recombination, tentatively assigned to a free-electron-to-acceptor transition (e, A), and to recombination of excitons trapped at known Bi-related states, marked T_2, T_3, and T_4. The shallow acceptor associated with the (e, A) transition is not known but could be carbon or some other impurity. The peaks marked T_3' and T_4' correspond to the phonon replicas of T_3 and T_4. In particular, T_2 is located in the shoulder of the (e, A) peak at 10 K and becomes slightly more pronounced at 30 K as the (e, A) peak decreases in intensity. The expected energies of transitions involving Bi-related states deeper within the band gap are marked as T_5-T_8. Emission from the T_5-T_8 states is likely weaker at low temperatures due to their low densities as well as the general inability of carriers to spatially migrate to lower-energy states by variable range hopping. Increasing the measurement temperature promotes additional detrapping and variable range-hopping events, leading to more efficient relaxation from higher-energy states to lower-energy states. The relatively low densities of the Bi-related bound states also allow them to be saturated under higher excitation power densities. Coupling detrapping with greater power densities forces recombination via excitons bound to neutral acceptors (A_0, X) that are at higher energies. Energy-transfer processes dominate by 80 K, and PL is mainly emitted in the form of a broad peak centered around the initial T_7 state energy. There is negligible PL from the T_2, T_3, and T_4 states. The sample with 0.26% Bi (not shown) behaves very similarly.

Photoluminescence from the sample with the next-highest Bi concentration, 0.33% [Fig. 1(b)], follows the same general trend, except that the (e, A) peak is not very strong at 10 K. The spectral weight also shifts to lower energy with increasing temperature and to higher energy with increasing power density, similar to the sample with 0.30% Bi. Yet, emission is enhanced from the T_3 through T_4' peaks relative to the (e, A) peak, especially with higher excitation powers. This is a consequence of higher densities of bound Bi-related states that accompany greater overall Bi concentrations and can be populated at the expense of shallow acceptor states.

To expand on the brief remark about the composition dependence of the T_i PL peaks above, we note that the energies of these features shift at a slower rate with composition than the band gap energy [18,30]. Both trends are shown in Fig. 2 along with the experimental values measured at 10 K. The band gap reduction in dilute bismide alloys is due to a strong upward movement of the VBE as well as a smaller, but still sizable, decrease in the CBE [30,31]. The Bi-related bound states, on the other hand, are expected to remain constant in energy in the band gap above the VBE of GaAs while the alloy VBE moves upward (see inset of Fig. 2). This is similar to the behavior of bound N pair states in $GaAs_{1-x}N_x$ [32]. Thus, the T_i peaks, resulting from CBE-to-T_i recombination, follow the decreasing trend of the CBE alone. By comparison, shallow acceptor states follow the VBE, and the associated (e, A) peak tracks the band gap energy (also shown in Fig. 2) [30].

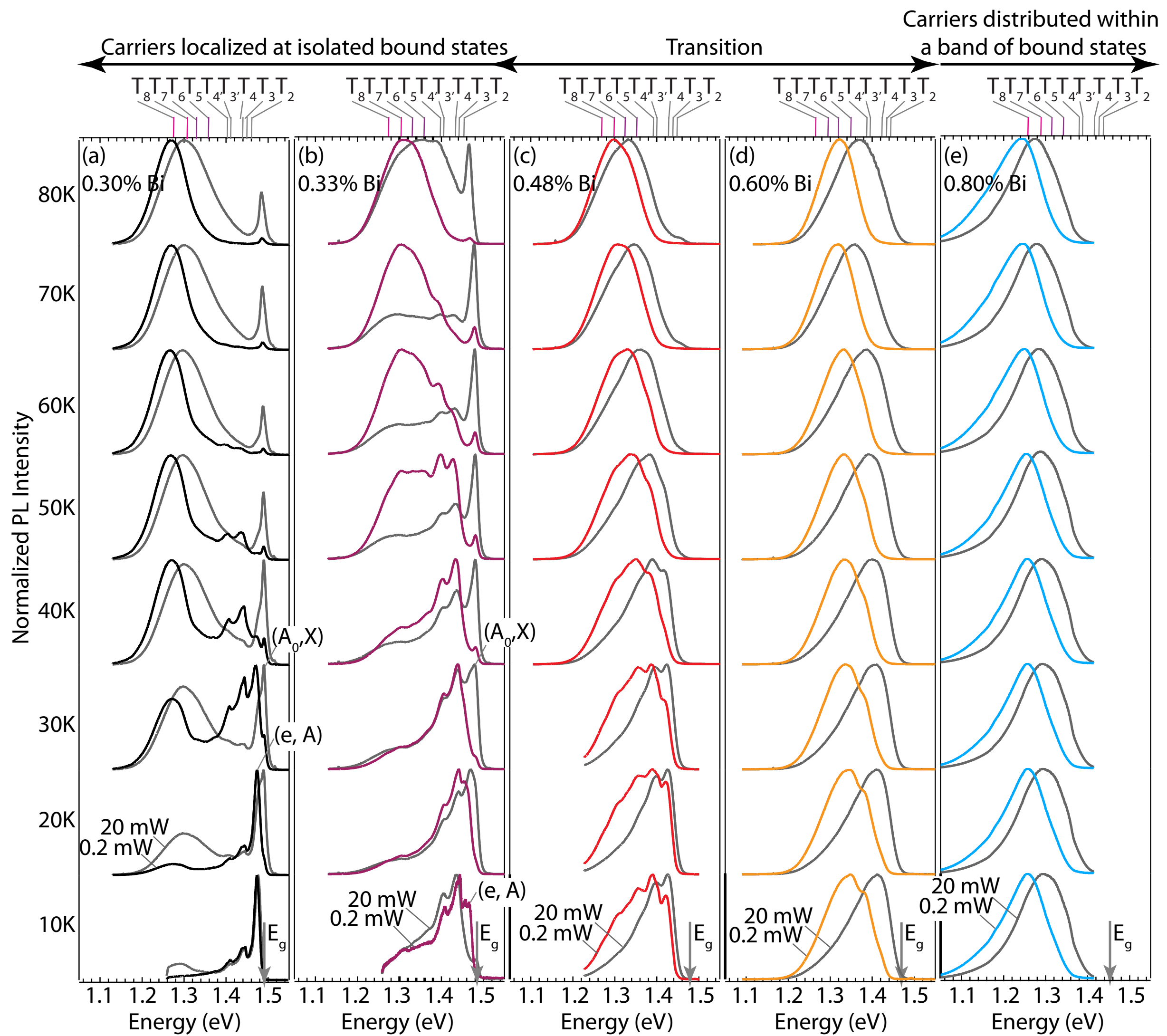

FIG. 1. Photoluminescence measurements as a function of temperature and excitation power for five representative samples with Bi concentrations of (a) 0.30%, (b) 0.33%, (c) 0.48%, (d) 0.60%, and (e) 0.80%. Spectra are normalized to peak values.

A change in the emission behavior becomes noticeable in the sample with 0.48% Bi [Fig. 1(c)]. Near-band-edge emission is no longer strongly excited at any temperature or even high excitation densities. Individual peaks also become washed out at temperatures >40 K in favor of a single broad band between T_2 and T_8 with a peak energy that continuously shifts to higher energies with excitation power. This trend is replicated in the sample with 0.60% Bi [Fig. 1(d)], where the individual peak features become even less distinguishable at lower temperatures. Finally, samples with ⩾0.80% Bi [Fig. 1(e) and those not shown] exhibit only one broad peak at all temperatures. It is typically at an energy near the expected T_7 and T_8 emission, and it shifts only slightly with temperature or excitation density. The evolution of this peak from the individual T_i states at 80 K is also shown in Fig. 2, where the shaded regions mark the peak full width at half maximum (FWHM). The temperature and composition dependence observed here suggests that at Bi concentrations >0.6%, there is enough overlap of shallower Bi-related states to facilitate efficient energy transfer to the very lowest energy states (with T_8 being the lowest distinct state identified).

Time-resolved PL measurements were performed to verify the *distribution* of localized and delocalized states contributing to the PL spectra as well as to further probe how carrier localization evolves with composition. Figure 3 displays the decay curves measured in samples spanning the intermediate Bi concentrations over which the PL progresses from T_i-dominated emission to a broad single peak. In each case, the PL decay times are fastest when measured at the high-energy end of the spectrum due to the relative ease with which carriers trapped at those states can also migrate to the lower-energy states. The radiative decay times are much longer from the lowest-energy states, where the holes are strongly trapped. A mobility edge, E_m, separates the localized and delocalized extremes [33]. The mobility edge energy was calculated for each sample by fitting the trend in the PL decay time vs

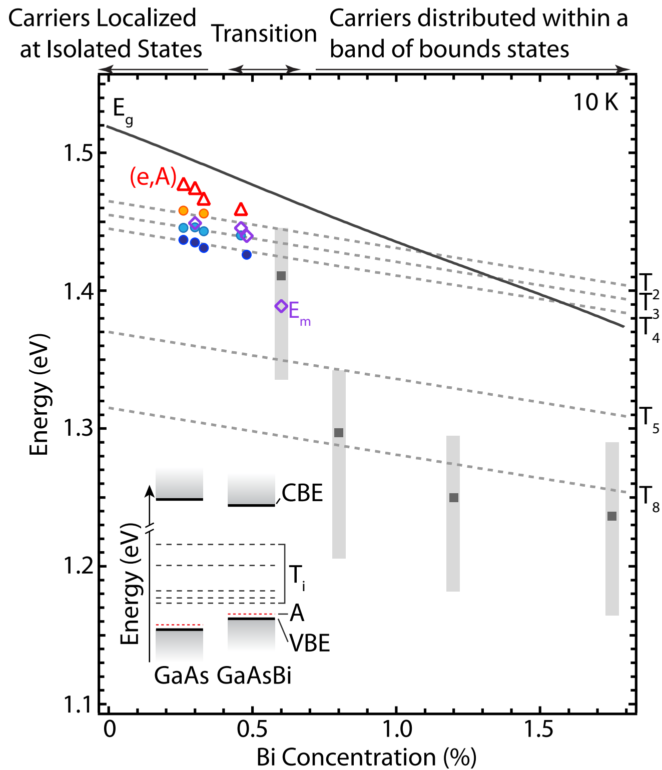

FIG. 2. PL peak energies as a function of Bi concentration measured at 10 K. The open triangles mark the $(e,\ A)$ peaks, while the closed circles mark the T_2–T_4 peaks. The closed squares mark the single broad PL peak energies, and the shaded regions denote their FWHM. The open diamonds correspond to the values of mobility edge, E_m, extracted from TRPL measurements. Inset schematic (bottom left) depicts the relative movements of the CBE, VBE, acceptor (A), and T_i levels as Bi is added to GaAs.

emission energy with the well-known form [34]

$$\tau(E) = \frac{\tau_R}{\{1 + \exp[\alpha(E - E_m)]\}}, \tag{1}$$

where τ_R is the radiative recombination time and α is a scaling factor. The experimentally derived decay times along with the fit according to Eq. (1) are displayed in Fig. 4, and the resulting values of E_m are marked in the spectra in Fig. 3. As expected, E_m decreases with increasing Bi concentration as the band gap energy drops and the spectral weight shifts to lower energies. More interestingly, the position of E_m relative to the peak position changes throughout this sample series. E_m resides above the T_3 and T_4 peaks in both samples with lower Bi concentration because the T_i states are not numerous enough to support efficient energy transfer to lower-energy states. However, once the PL begins to transition to a single broad peak (0.60% Bi), E_m shifts toward the center of the peak. This behavior is consistent with emission from a continuous distribution of states with progressively more localization when moving to lower energies. The location of E_m above the peak energy in the broad PL band of the sample with 0.60% Bi indicates that most excitons that contribute to it (especially on the low-energy side) are localized to a similar degree to those trapped at distinct T_i states at low Bi concentrations. Thus, the continuous distribution of Bi-derived states effectively funnels trapped excitons to the deepest ones.

The *extent* of exciton localization behavior was confirmed through the influence of a magnetic field on the emission from the bound states. Magnetic fields induce a change in the electron and hole motion and therefore a change in the energy of the excitonic state. This results in a diamagnetic blueshift of the PL peak energy, ΔE_d, with increasing magnetic field. In the "low-field" limit ($B < 10\,\mathrm{T}$ for our samples), ΔE_d is dependent on the exciton reduced mass, μ, and root-mean-square (rms) radius of the exciton, $\sqrt{\langle r_\perp^2 \rangle}$, as [35]

$$\Delta E_d = \frac{e^2 r_\perp^2}{8\mu} B^2 = \sigma B^2. \tag{2}$$

The exciton reduced mass is expressed as $\mu = (m_e^{-1} + m_h^{-1})^{-1}$, where m_e and m_h are the electron and hole masses, respectively. σ is the diamagnetic shift coefficient. Thus, the diamagnetic shift in the low-field limit can provide an indication of the *size* of the exciton. Similar analyses have been previously used to evaluate exciton localization in disordered potentials, within low-dimensional quantum structures and at bound isoelectronic N impurity-related states (see for example Refs. [36] and [37] and references therein). Here, we use it as a further indicator of how localization evolves from the distinct T_i states observed in samples with low Bi concentration to the broad single peak observed in samples with higher Bi concentrations.

Magneto-PL measurements were performed on two samples with 0.30 and 0.80% Bi to examine the two regimes of localization behavior. The magneto-PL spectra of these two samples are displayed in Figs. 5(a) and 5(b), and the zero-field PL peak energies are marked in Fig. 5(c). Specifically, we followed the diamagnetic shift of the T_3 peak of the sample with 0.30% Bi and the broad peak of the sample with 0.80% Bi. The PL peak energies as a function of magnetic field are plotted in Figs. 5(d) and 5(e) along with the $(A_0,\ X)$ peak of GaAs (spectra not shown).

Qualitatively, the two $GaAs_{1-x}Bi_x$ samples exhibit trends in ΔE_d that are more similar to each other than that of GaAs. Based on Eq. (2), the excitons associated with the T_3 peak in samples with lower Bi concentrations and the broad PL peak at higher Bi concentrations both have a much smaller radius than that found in GaAs, in line with our expectation that they are localized [36]. The values of σ extracted from fitting the low-field data points [Fig. 5(e)] to Eq. (2) are listed in Table I. The values of μ were extracted by fitting the full range of magnetic-field data, including those measured well into the high-field limit $>15\,\mathrm{T}$, using a numerical method [38].This approach has been used routinely to determine μ in $GaAs_{1-x}N_x$ and $GaAs_{1-x}Bi_x$ alloys [19,39,40]. They are also listed in Table I. Reference [19] reported an increase in μ with Bi concentration in $GaAs_{1-x}Bi_x$ alloys with up to 6% Bi. Those measurements were performed on free excitons at 200 K, where the holes were assumed not to be localized. Our results follow a similar trend, but the values of μ measured here for similar Bi concentrations are slightly higher. As discussed in Ref. [23], this discrepancy is due to enhanced local compressive strain experienced by the trapped exciton in the immediate vicinity of the Bi pair. Using σ and μ,

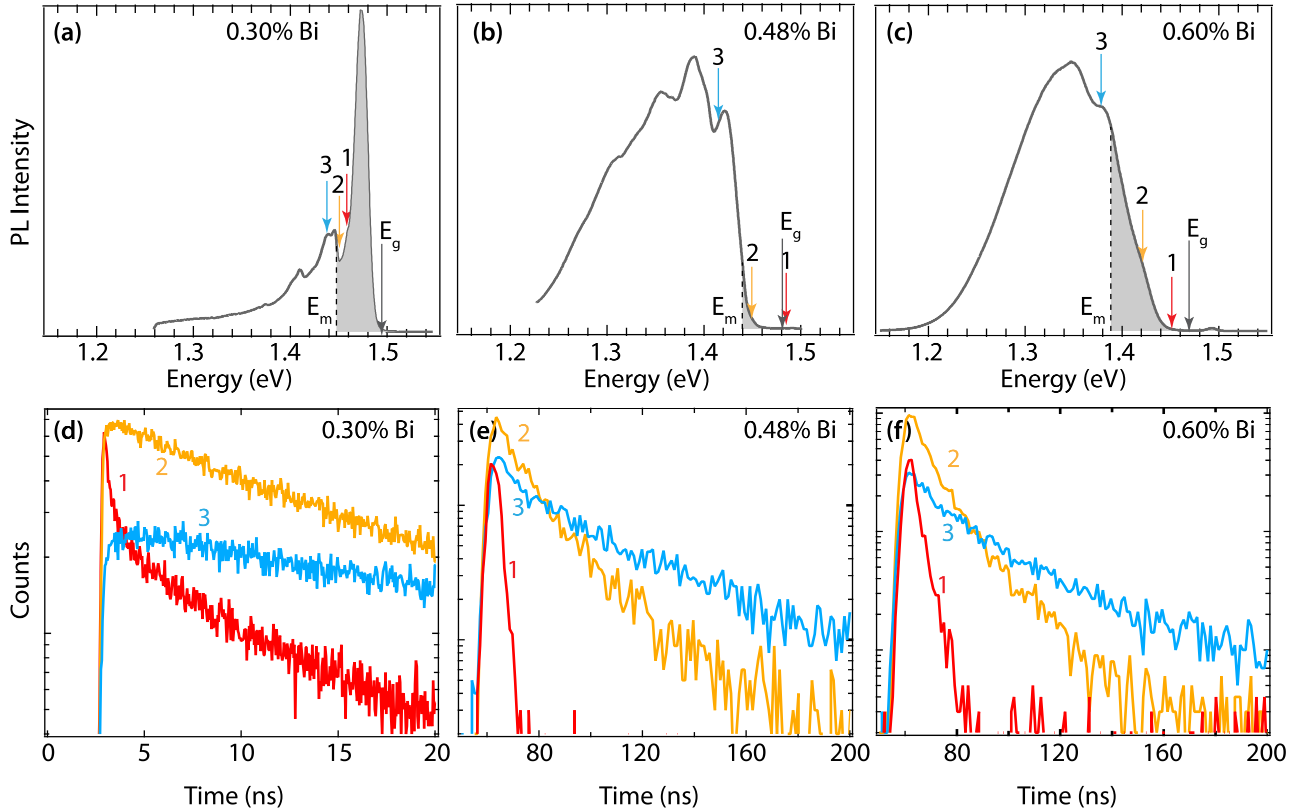

FIG. 3. Time-resolved PL measurements measured at 5 K. (a)–(c) PL spectra displayed for three samples with 0.30, 0.48, and 0.60% Bi, respectively. (d)–(f) PL decay curves displayed for samples (a)–(c). The decay curves were measured at the energies marked with the corresponding numbers in the spectra. The mobility edge, E_m, extracted from Eq. (1) and the band gap, E_g, are also marked in each spectrum.

we then calculate the rms radius $\sqrt{\langle r_\perp^2 \rangle}$ for those excitons involved in the PL transitions followed in each sample. These values are additionally listed in Table I. The radius decreases from 14.2 nm for shallow acceptor-bound excitons in GaAs to 10.6 and 9.4 nm for excitons bound to Bi-derived states in $GaAs_{1-x}Bi_x$ with 0.30 Bi and 0.80% Bi, respectively. The key takeaway from these measurements is that excitons recombining from the broad distribution of states that contribute to the single PL peak observed in the sample with 0.80% Bi are even slightly more spatially localized than the excitons trapped at the T_3-related states in the sample with 0.30% Bi.

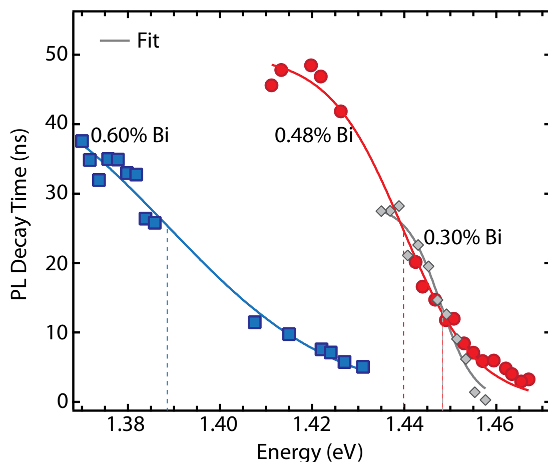

FIG. 4. PL decay times as a function of energy for the three samples shown in Fig. 3: 0.30% Bi (diamonds), 0.48% Bi (circles), and 0.60% Bi (squares). Solid lines show the fits to the data points. The mobility edge values extracted from the fits are marked with vertical dashed lines.

IV. DISCUSSION

While the existence of hole localization is already well documented in $GaAs_{1-x}Bi_x$ alloys with Bi concentrations <0.5% Bi and >2% Bi [18,21,22,30], this work clearly and systematically shows the transition between these two regimes. The results indicate that that there is a relatively rapid shift in the carrier localization behavior in $GaAs_{1-x}Bi_x$ as the Bi concentration is increased. Below ~0.4% Bi, individual Bi-related bound states play a large role in hole localization, especially at the lowest temperatures where hopping-mediated energy transfer to lower-energy states is limited. Above ~0.6% Bi, overlap of these states allows holes to easily find the deepest ones. The demarcation between these regimes is evident in the plot of PL peak vs alloy concentration in Fig. 6. Between 0.8 and 1.75% Bi, the 10 K PL peak is located ⩾150 meV below the band gap, which represents a substantial degree of localization.

The evolution in the localization behavior found here is qualitatively similar to that observed in $GaAs_{1-x}N_x$ alloys [11,12]. In that system, an increase in the concentration of

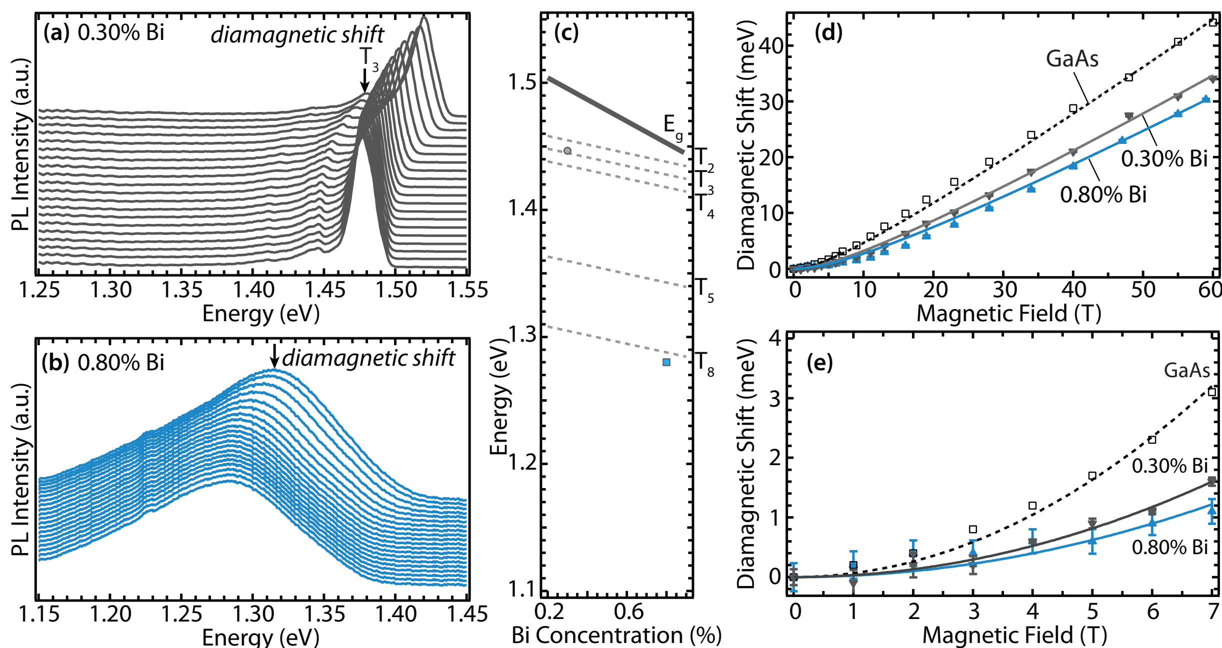

FIG. 5. PL spectra measured at 1.5 K in magnetic fields up to 58 T for representative samples with Bi concentrations of (a) 0.30% and (b) 0.80%. (c) Zero-field PL peak energies for both samples. The diamagnetic shift of the PL peaks for both dilute bismide samples and the (A_0, X) peak of GaAs (spectra not shown) for the full range of magnetic fields (d) and the low-field region (e) are also displayed.

N-related bound states allows the wave function of localized excitons to overlap adjacent pair states and permits fast transfer of electrons to lower-lying isolated states in the band gap. A single broad PL peak formed once the CBE had moved downward through the N-related bound states (∼0.4% N). However, the broad PL band in $GaAs_{1-x}N_x$ is only located approximately 50 meV below the band gap and closely follow the band gap trend with composition by 0.4% N. Thus, $GaAs_{1-x}Bi_x$ experiences an intermediate stage where energy transfer to very deep states becomes efficient at compositions well below where these states eventually merge with the valence-band edge. This intermediate stage is not readily observed in $GaAs_{1-x}N_x$, and it leads to much stronger localization than $GaAs_{1-x}N_x$ over a composition range of several percent Bi.

We argue here that the origin of the strong localization in $GaAs_{1-x}Bi_x$ is due to the deeper localized states that Bi-Bi interactions produce. Along with the experimentally determined PL peak energies, Fig. 6 displays the expected trends of the conduction-band-to-T_i-state energies as a function of alloy composition. We have additionally included the PL peak energy and FWHM information from samples with higher Bi concentrations reported in the literature [19,20,41]. Overall, the PL peak energy appears to be pinned by the T_8 state out to concentrations near 6%, at which point the valence band is expected to overtake it. The lone data point past 8% Bi suggests that the PL peak energy then follows the band gap (within ∼50 meV), similar to $GaAs_{1-x}N_x$ [11].

The deep localization behavior in $GaAs_{1-x}Bi_x$ is therefore a consequence of two factors: the existence of a Bi-related state located well above the VBE and the relatively slow upward motion of the valence-band edge with composition. Together, they result in the valence band overtaking the

TABLE I. Parameters extracted from the diamagnetic shift data in Fig. 5.

%Bi	σ (meV/T^2)	μ (m_0)	$\sqrt{\langle r_\perp^2 \rangle}$ (nm)
0	65.3	0.060	14.2
0.30	32.6	0.075	10.6
0.80	24.8	0.079	9.4

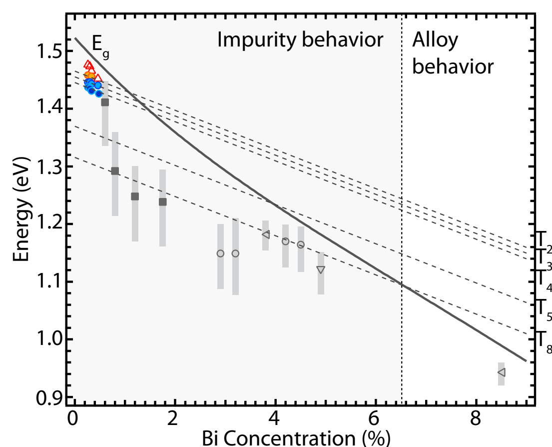

FIG. 6. PL peak energies as a function of Bi concentration. The right-side-up triangles, closed circles, and closed squares are data from this study (also shown in Fig. 2) The FWHM of the peaks are marked with shaded regions. Data marked with open circles are from Ref. [20], the data marked with left-pointing triangles are from Ref. [19], and the data point marked with an open upside-down triangle is from Ref. [41].

Bi-related states at much higher Bi concentrations than in $GaAs_{1-x}N_x$, leading to a wider range of compositions in which there exist deeply bound states to trap holes. We note that the slight offset in the PL peak energy from the T_8 state in the samples with concentration between ~0.8 and ~3% may be the consequence of a couple of experimentally observed factors. One is the propensity of the PL peak to shift to slightly lower energies under low-excitation densities as fewer bound states are filled [see Fig. 1(e)]. Excitation powers used by other groups may vary compared to ours. The other factor is spatial fluctuation in the CBE due to alloying, which will produce regions where the CBE is lower.

Identification of the origin of the localization in $GaAs_{1-x}Bi_x$ allows us to further understand the consequences for the alloy properties and performance. First, deep localization behavior appears to be an inherent property of $GaAs_{1-x}Bi_x$ with $0.4\% < \mathrm{Bi} < 6\%$ rather than primarily a function of the overall material quality or growth conditions. This conclusion is underscored by the fact that samples grown by multiple groups follow the same general trend [19,20]. It implies that improving the synthesis of $GaAs_{1-x}Bi_x$ and reducing defect densities will not necessarily result in significantly reduced localization in alloys within this composition range. Second, the localization energy is lowered once the VBE overtakes the T_8 state at concentrations around 6% Bi. Importantly, this suggests that the alloy should behave more regularly above this concentration, where VBE and CBE fluctuations are the main source of localization. This is consistent with other trends observed in $GaAs_{1-x}Bi_x$ [19,42]. For example, μ was found to rise to unexpectedly high values for Bi concentrations in the range of 1–6% before dropping once the Bi concentration reached 8% [19]. Theoretically, the VBE was also found to be less affected by atomistic randomness at Bi concentrations $\geqslant 8\%$ [42]. By determining that exciton localization is dominated by the T_8 state, we can better predict the localization behavior in dilute $GaAs_{1-x}Bi_x$ alloys as a function of composition. A particular consequence is that applications that require Bi concentrations lower than that will always have to tolerate higher degrees of localization or potential fluctuations, which can lower carrier mobility and transport.

ACKNOWLEDGMENTS

This work was authored in part by the National Renewable Energy Laboratory, operated by Alliance for Sustainable Energy, LLC, for the US Department of Energy (DOE) under Contract No. DE-AC36-08GO28308. Funding was provided by the US DOE, Office of Science, Basic Energy Sciences Office (Novel Semiconductors program). Measurements at the NHMFL LANL were supported by Grant No. NSF-DMR-1157490, and the State of Florida.

The views expressed in the article do not necessarily represent the views of the Department of Energy or the U.S. Government. The US Government retains and the publisher, by accepting the article for publication, acknowledges that the US Government retains a nonexclusive, paid-up, irrevocable, worldwide license to publish or reproduce the published form of this work, or allow others to do so, for US Government purposes.

[1] M. Weyers, M. Sato, and H. Ando, Jpn. J. Appl. Phys., Part 1 **31**, L853 (1992).
[2] J. D. Perkins, A. Mascarenhas, Y. Zhang, J. F. Geisz, D. J. Friedman, J. M. Olson, and S. R. Kurtz, Phys. Rev. Lett. **82**, 3312 (1999).
[3] W. Shan, W. Walukiewicz, J. W. Ager, E. E. Haller, J. F. Geisz, D. J. Friedman, J. M. Olson and S. R. Kurtz, Phys. Rev. Lett. **82**, 1221 (1999).
[4] S. Francoeur, M.-J. Seong, A. Mascarenhas, S. Tixier, M. Adamcyk, and T. Tiedje, Appl. Phys. Lett. **82**, 3874 (2003).
[5] B. Fluegel, S. Francoeur, A. Mascarenhas, S. Tixier, E. C. Young, and T. Tiedje, Phys. Rev. Lett. **97**, 067205 (2006).
[6] C. A. Broderick, M. Usman, S. J. Sweeney, and E. P. O'Reilly, Semicond. Sci. Technol. **27**, 094011 (2012).
[7] C. Pashartis and O. Rubel, Phys. Rev. Appl. **7**, 064011 (2017).
[8] Y. Zhang and A. Mascarenhas, Phys. Rev. B **61**, 15562 (2000).
[9] P. R. C. Kent and A. Zunger, Phys. Rev. Lett. **86**, 2613 (2001).
[10] F. Esser, S. Winnerl, A. Patane, M. Helm, and H. Schneider, Appl. Phys. Lett. **109**, 182113 (2016).
[11] K. Alberi, B. Fluegel, D. A. Beaton, A. J. Ptak, and A. Mascarenhas, Phys. Rev. B **86**, 041201(R) (2012).
[12] B. Fluegel, K. Alberi, D. A. Beaton, S. A. Crooker, A. J. Ptak, and A. Mascarenhas, Phys. Rev. B **86**, 205203 (2012).
[13] J. A. Kash, H. Mariette, and D. J. Wolford, Phys. Rev. B **32**, 3753 (1985).
[14] Y. Zhang, A. Mascarenhas, and L.-W. Wang, Phys. Rev. B **71**, 155201 (2005).
[15] K. Alberi, D. A. Beaton, and A. Mascarenhas, Phys. Rev. B **92**, 241201(R) (2015).
[16] S. Francoeur, S. Tixier, E. Young, T. Tiedje, and A. Mascarenhas, Phys. Rev. B **77**, 085209 (2008).
[17] G. Ciatto, E. C. Young, F. Glas, J. Chen, R. A. Mori, and T. Tiedje, Phys. Rev. B **78**, 035325 (2008).
[18] M. Usman, C. A. Broderick, A. Lindsay, and E. P. O'Reilly, Phys. Rev. B **84**, 245202 (2011).
[19] G. Pettinari, A. Polimeni, J. H. Blokland, R. Trotta, P. C. M. Christianen, M. Capizzi, J. C. Maan, X. Lu, E. C. Young, and T. Tiedje, Phys. Rev. B **81**, 235211 (2010).
[20] M. K. Shakfa, K. Jandieri, M. Wiemer, P. Ludewig, K. Volz, W. Stolz, S. D. Baranovskii, and M. Koch, J. Phys. D: Appl. Phys. **48**, 425101 (2015).
[21] R. Kudrawiec, M. Syperek, P. Poloczek, J. Misiewicz, R. H. Mari, M. Shafi, M. Henini, Y. Galvao Gobato, S. V. Novikov, J. Ibanez, M. Schmidbauer, and S. I. Molina, J. Appl. Phys. **106**, 023518 (2009).
[22] S. Imhof, C. Wagner, A. Thranhardt, A. Chernikov, M. Koch, N. S. Koster, S. Chatterjee, S. W. Koch, O. Rubel, X. Lu, S. R. Johnson, D. A. Beaton, and T. Tiedje, Appl. Phys. Lett. **98**, 161104 (2011).

[23] K. Alberi, T. M. Christian, B. Fluegel, S. A. Crooker, D. A. Beaton, and A. Mascarenhas, Phys. Rev. Mater. **1**, 024605 (2017).

[24] A. J. Ptak, R. France, D. A. Beaton, K. Alberi, J. Simon, A. Mascarenhas, and C.-S. Jiang, J. Cryst. Growth **338**, 107 (2012).

[25] X. Lu, D. A. Beaton, T. Tiedje, R. Lewis, and M. B. Whitwick, Appl. Phys. Lett. **92**, 192110 (2008).

[26] R. Bastiman, A. R. B. Mohmad, J. S. Ng, J. P. R. David, and S. J. Sweeney, J. Cryst. Growth **338**, 57 (2012).

[27] D. L. Sales, E. Guerrero, J. F. Rodrigo, P. L. Galindo, A. Yaez, M. Shafi, A. Khatab, R. H. Mari, M. Henini, S. Novikov, M. F. Chisholm, and S. I. Molina, Appl. Phys. Lett. **98**, 101902 (2011).

[28] S. Mazzucato, P. Boonpeng, H. Carrere, D. Lagarde, A. Arnoult, G. Lacoste, T. Zhang, A. Balocchi, T. Amand, X. Marie, and C. Fontaine, Semicond. Sci. Technol. **28**, 022001 (2013).

[29] D. A. Beaton, A. Mascarenhas, and K. Alberi, J. Appl. Phys. **118**, 235701 (2015).

[30] T. M. Christian, K. Alberi, D. A. Beaton, B. Fluegel, and A. Mascarenhas, Jpn. J. Appl. Phys. **56**, 035801 (2017).

[31] R. Kudrawiec, J. Kopaczek, M. P. Polak, P. Scharoch, M. Gladysiewicz, J. Misiewicz, R. D. Richards, F. Bastima, and J. P. R. David, J. Appl. Phys. **116**, 233508 (2014).

[32] Y. Zhang, A. Mascarenhas, J. F. Geisz, H. P. Xin, and C. W. Tu, Phys. Rev. B **63**, 085205 (2001).

[33] M. Oueslati, C. Benoit, and M. Zouaghi, Phys. Rev. B **37**, 3037 (1988).

[34] R. A. Mair, J. Y. Lin, H. X. Jiang, E. D. Jones, A. A. Allerman, and S. R. Kurtz, Appl. Phys. Lett. **76**, 188 (2000).

[35] N. Miura, *Physics of Semiconductors in High Magnetic Fields* (Oxford University Press, New York, 2008).

[36] M. Erdmann, C. Ropers, M. Wenderoth, R. G. Ulbrich, S. Malzer, and G. H. Dohler, Phys. Rev. B **74**, 125412 (2006).

[37] Y. Harada, T. Kubo, T. Inoue, O. Kojima, and T. Kita, J. Appl. Phys. **110**, 083522 (2011).

[38] D. Cabib, E. Fabri, and G. Fiorio, Solid State Commun. **9**, 1517 (1971).

[39] G. Pettinari, A. Polimeni, M. Capizzi, J. H. Blokland, P. C. M. Christianen, J. C. Maan, E. C. Young, and T. Tiedje, Appl. Phys. Lett. **92**, 262105 (2008).

[40] F. Masia, A. Polimeni, G. Baldassarri Hoger von Hogersthal, M. Bissiri, P. J. Klar, and W. Stolz, Appl. Phys. Lett. **82**, 4474 (2003).

[41] M. A. G. Balanta, K. Kopaczek, V. Orsi Gordo, B. H. B. Santos, A. D. Rodrigues, H. V. A. Galeti, R. D. Richards, F. Bastiman, J. P. R. David, R. Kudrawiec, and Y. Galvao Gobato, J. Phys. D: Appl. Phys. **49**, 355104 (2016).

[42] M. Usman, C. A. Broderick, Z. Batool, K. Hild, T. J. C. Hosea, S. J. Sweeney, and E. P. O'Reilly, Phys. Rev. B **87**, 115104 (2013).